*International Journal of Thermophysics, Vol. 19, No. 2, 1998*

# Small-Angle Neutron Scattering Studies of Vesicle Stability[1]

**J. T. Mang[2] and R. P. Hjelm[2, 3]**

Small-angle neutron scattering (SANS) was used to investigate the structure of mixed colloids of egg yolk phosphatidylcholine (EYPC) with the bile salt, cholylglycine (CG), in $D_2O$ as a function of pressure ($P$) and temperature ($T$). At atmospheric pressure, the system forms an isotropic phase of mixed, single-bilayer vesicles (SLVs). Increasing the external hydrostatic pressure brought about significant changes in particle morphology. At $T = 25°C$, application of a pressure of 3.5 MPa resulted in collapse of the SLVs. A further increase in $P$, up to 51.8 MPa, resulted in a transition from a phase of ordered (stacked), collapsed vesicles to one of stacked, ribbon-like particles. A similar collapse of the vesicles was observed at a higher temperature ($T = 37°C$) with increasing $P$, but at this temperature, no ribbon phase was found at the highest pressure explored.

**KEY WORDS:** small-angle neutron scattering; stability; vesicles.

## 1. INTRODUCTION

In recent years, there has been considerable interest the stability of bilayer vesicles formed by mixed surfactant systems [1–3]. This work has largely considered the effects of packing due to molecular geometrical factors and the effect of the bending elastic modulus. This assumption is embodied in the work of Israelachvilli [4] and also of Safran et al. [1]. In the latter work, Safran, et al. considered the curvature free energy and showed that, with the introduction of a second molecular species, the composition of each monolayer of the bilayer provides an additional degree of freedom

[1] Paper presented at the Thirteenth Symposium on Thermophysical Properties, June 22–27, 1997, Boulder, Colorado, U.S.A.

[2] Manuel Lujan Jr. Neutron Scattering Center, Los Alamos National Laboratory, Los Alamos, New Mexico 87545-1663, U.S.A.

[3] To whom correspondence should be addressed.



0195-928X/98/0300-0461$15.00/0 

that can give rise to effective negative values of the curvature free energy for vesicles, making them stable with respect to flat lamellae. These studies consider mixed bilayers as incompressible; thus, the effects of pressure on vesicle stability are not explicitly considered. The expression for the free energy for shapes of closed fluid lipid–bilayer membranes, including vesicles relative to planar lamellae derived by Zhong-can and Helfrich [5] as well as others includes pressure as well as the energy of curvature,

$$F_c = \tfrac{1}{2}K_c \int (c_1 + c_2 - c_0)^2 \, dA + \Delta p \int dV + \gamma' \int dA \tag{1}$$

Here $K_c$ is the bending modulus, $c_1$ and $c_2$ are the principal curvatures of the interface, and $c_0$ is the spontaneous curvature. $\Delta p (= p_i - p_e)$ represents a pressure gradient between the interior of the membrane and the surrounding fluid, while $\gamma'$ represents the surface tension or surface energy density. In this model, the pressure gradient plays an integral role in determining particle stability. For example, in considering a simple particle morphology such as a spherical vesicle of average curvature $R^{-1}$, minimization of $F_c$ requires

$$\Delta p \sim \frac{2\gamma'}{R}$$

which is just the classic Young–Laplace (Y-L) equation for soap bubbles.

While Eq. (1) has been successful in predicting the equilibrium shapes of membrane systems, there has been considerable controversy [4, 6, 7] about the physical origin of the last two terms, which appear in the expression. These terms enter into the Helfrich formalism as Lagrange multipliers to satisfy the conditions of constant volume and area, but they may represent real work contributions to the free energy. This result, however, was originally derived to describe macroscopic systems, and as Tanford [6] originally pointed out, vesicles are permeable to water; thus, it is difficult to understand how a hydrostatic pressure gradient can be maintained. So, too, is the possibility of an osmotic gradient, which would require an excess amount of solute (salt, for example) to be trapped at the interior. While a small gradient may be possible when the vesicles are formed by mechanical means (sonification), such a gradient is unlikely when the vesicles form spontaneously, as in the present case. Further, it is unclear whether such concepts as surface tension apply on the microscopic level [8, 9].

Mixed surfactant systems form vesicles of definite size and shape. If there is no pressure gradient across the curved interface, and there is no surface tension, then what holds these membranes together? We may not

be able to define a surface tension or a pressure gradient in the macroscopic sense for these systems; however, the forces involved in binding the membranes may appear as effective pressures and surface tensions. So, while the mathematical formalism is sound, a reinterpretation of the work terms may be needed.

In studying the stability of membrane systems, then, it is important to be able to quantify these forces no matter what their origin. By varying the external hydrostatic pressure according to the Y-L interpretation, we may reach a point where the applied pressure exceeds the effective pressure of the membranes, forcing them to collapse. The point of collapse then will provide valuable information on the magnitude of the forces which act on these systems. In order to elucidate the role of pressure in determining the stability criteria for colloids of mixed surfactant systems, we performed small-angle neutron scattering (SANS) measurements on particle morphology as a function of the pressure of bile salt (cholylglycine)/egg yolk phosphatidylcholine (EYPC) mixtures in the region of the isotropic (I) phase.

## 2. MATERIALS AND METHODS

### 2.1. System

CG/EYPC samples were prepared by dissolving purified EYPC (Sigma, Type VIII-E) and sodium glycocholate (Sigma Chemical Co.) in ethanol and then mixing the two components at a molar ratio (EYPC/BS) of $\Gamma^{-1} = 0.8$. After vacuum-drying, the preparation was dissolved in a $D_2O$ buffer containing 0.15 $M$ NaCl with Tris buffer (pH 7.5) to make a stock solution containing a 50 mg/ml total lipid concentration. The samples (2 mg/ml) were prepared by further dilution with $D_2O$ buffer and allowed to equilibrate for $\sim 2$ days in the dark. The final concentration corresponded to the mixed, spherical single-bilayer vesicle (SLV) portion of the phase diagram.

### 2.2. Small-Angle Neutron Scattering

SANS measurements were performed at the Intense Pulsed Neutron Source at Argonne National Laboratory, employing the Small-Angle Neutron Diffractometer (SAD), and at the Cold Neutron Research Facility (CNRF) of the National Institute of Standards and Technology (NIST), employing the NG3 beamline. On SAD, scattering data were acquired using the time-of-flight method [10]. At NIST, neutrons of wavelength 5 Å ($\Delta\lambda/\lambda = 0.15$) and two camera settings were used. In both cases, the raw

data were corrected for empty cell, background, and buffer scattering. In order to interpret the data, a nonlinear least-squares procedure was used to fit the measured lineshapes to the expected scattering of different model systems.

Neutron scattering experiments measure the scattering intensity, $I(Q)$, as the absolute differential cross section per unit scattering mass ($cm^2 \cdot mg^{-1}$) as a function of the magnitude of the scattering vector, $Q$, which is related to the incident neutron wavelength, $\lambda$, and the scattering angle, $2\theta$, by $Q = (4\pi/\lambda) \sin \theta$. The scattered neutron intensity, for a system of $N$ particles of volume, $V$, and uniform scattering length density, dispersed in a uniform solvent, can be expressed as

$$I(Q) = \frac{N}{M} V^2 (\Delta\rho)^2 \langle P(\mathbf{Q})\, S(\mathbf{Q}) \rangle$$

where $P(\mathbf{Q})$ is the normalized form factor of a single particle and is given as $P(\mathbf{Q}) = |F(\mathbf{Q})|^2$. $F(\mathbf{Q})$ is the Fourier transform of the particle structure given as the variation of scattering length density, $\rho(\mathbf{r})$, as a function of position, $r$, in the sample. $S(\mathbf{Q})$ is the structure factor, which accounts for interparticle correlations, and $M$ is the mass of the particle. $\Delta\rho$ is the scattering length density contrast between the average scattering length density of the particle, $\overline{\rho_p}$, and the solvent, $\rho_s$, $\Delta\rho = \overline{\rho_p} - \rho_s$. Table I summarizes the particle form factors which are relevant to this work. In the table, $j_1$ is the first-order spherical Bessel function, $R$ is the outer radius of the vesicle, and $r$ is the inner radius. $l_T$ is the hydrocarbon tail thickness (of EYPC), $2l$ is the bilayer thickness, $L = 2 \cdot (l + l_T)$, and $2l_y$ represents the width of a ribbon. $\Delta\rho_H$ is the scattering length contrast between the EYPC headgroup

**Table I.** Particle Form Factors for the Structural Models used in this Study[a]

| Model | Particle form factor, $P(\mathbf{Q})$ |
|---|---|
| Single-layer vesicle | $\frac{9}{Q^2(R^3 - r^3)^2} [R^2 j_1(QR) - r^2 j_1(Qr)]^2$ |
| Infinite sheet | $\frac{P_z(Q)}{Q^2}$, $F_z(Q) \equiv \left[ \frac{2l\,\Delta\rho_H}{L\,\overline{\Delta\rho}} \operatorname{sinc}(Ql) + \frac{2l_T\,\Delta\rho_{TH}}{L\,\overline{\Delta\rho}} \operatorname{sinc}(Ql_T) \right]$ |
| Infinite ribbon | $\frac{\lvert F_z(Q_k) \operatorname{sinc}(Q_l l_y) \rvert^2}{Q_l}$ |

[a] SS model (as described in the text) consists of the powder average of an infinite sheet multiplied by the structure factor for a 1-D lattice. In the SR model, $P(\mathbf{Q})$ for an infinite ribbon replaces that of an infinite sheet.

and the solvent and $\Delta\rho_{TH}$ is the contrast between the EYPC tail region and the headgroup.

## 3. RESULTS

The results of SANS measurements of the CG/EYPC system over the range of pressures explored ar $T = 25°C$ are shown in Fig. 1, where the curves have been shifted along the vertical axis for clarity. Dramatic changes in the measured scattering curves were seen with increasing pressure. At atmospheric pressure ($P = 0.1$ MPa), the data are consistent with the presence of mixed SLVs, as expected from the known phase diagram [11]. At elevated pressures there is the appearance of a Bragg peak centered at $Q_0 = 0.123\ \text{Å}^{-1}$ ($1.23\ \text{nm}^{-1}$), corresponding to a bilayer spacing, $d$, of 51 Å. Pressure-dependent changes were observed in the falloff at low $Q$. The appearance of the single Bragg peak suggests the presence of stacking order in the system at high pressures, while the change in slope of the low $Q$ data suggests a change in the fundamental stacked unit with pressure.

Results of model calculations along with the measured data are shown in Fig. 2 for several pressures. As shown in Fig. 2a, the data obtained at

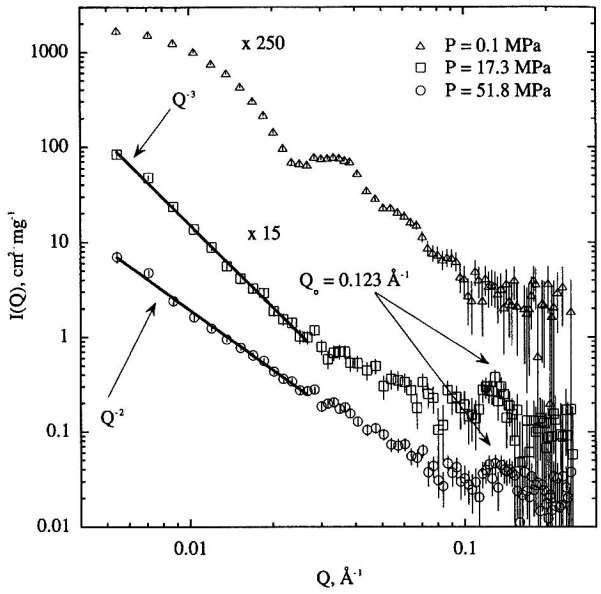


**Fig. 1.** SANS measurements of the CG/EYPC system (EYPC/BS = 0.8, $2\ \text{mg} \cdot \text{ml}^{-1}$) as a function of pressure.

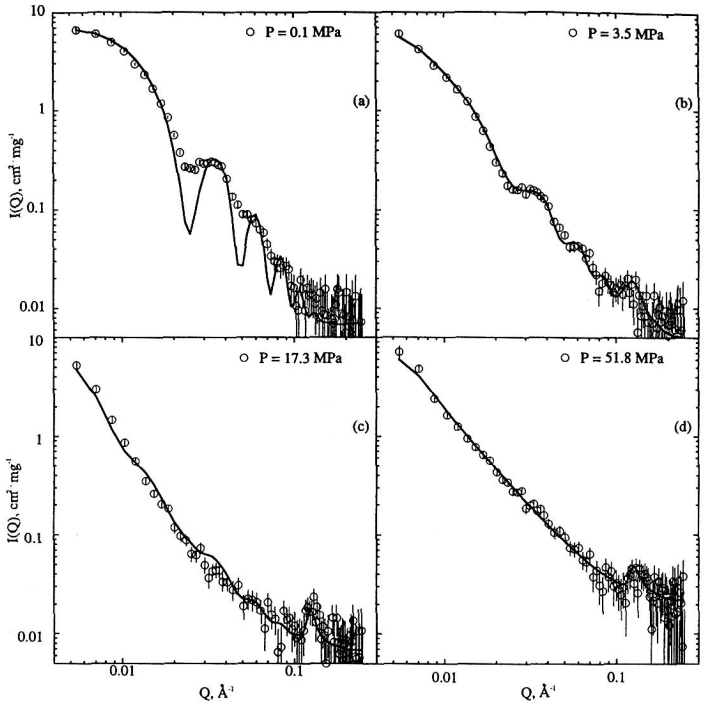


**Fig. 2.** SANS measurements as a function of pressure ($T = 25°C$). The solid lines are fits to model systems as described in the text. With increasing pressure, the system transformed from an isotropic phase of SLVs to a phase of stacked ribbon-like particles.

atmospheric pressure can be readily modeled as a system of mixed SLVs. The solid line in Fig. 2a is the result of a fit of the data to the particle form factor for an SLV with $R = 147$ Å and thickness $t = 35$ Å. Deviations of the model from the measured data at the minima are likely due to a small amount of polydispersity and/or multiple scattering. The solid line in Fig. 2d is the result of a fit of the data to a model consisting of stacked infinite ribbon-like (SR) particles, 30 Å thick, 25 Å wide, and with a stack height, $M$, of 13. Attempts to model the data as stacks of infinite sheets failed to describe our data accurately, as randomly oriented infinite sheet scattering falls off as $Q^{-4}$ at low $Q$ and produces a Bragg peak that is several orders of magnitude too small. At the intermediate pressures, the slopes of the scattering curves in the low-$Q$ region suggest a coexistence region of ribbons with infinite sheets. In Figs. 2b and c, the solid lines are the result of fits of the data to a linear combination of the SLV, SR, and

stacked infinite sheet (SS) models. Best fits were obtained with infinite sheets of 30-Å thickness. At $P = 3.5$ MPa, $M = 5$, while for higher pressures, $M = 13$ gave the best results. Such a coexistence has been seen previously in electron micrograph studies of native bile [12].

Scattering curves measured at 37°C as a function of pressure are shown in Fig. 3. As in the previous data (Figs. 1 and 2), significant changes occurred upon increasing pressure. For $P < 5.0$ MPa (Fig. 3) the data are well described by the form factor for an SLV with $R = 170$ Å and $t = 40$ Å. At higher pressures, the curves fall off more rapidly in the low-$Q$ region, while the maxima arising from the SLV contribution decreased. For all pressures, the scattering curves overlay above $Q = 0.04$ Å$^{-1}$. This suggests that the transition is not complete and that the contribution from the new phase, while dominating at low $Q$, falls off quickly.

The value of $\sim 2$ for the slope at low $Q$ again suggests the presence of sheet-like structures. But in contrast to the data collected ar $T = 25$°C, no distinct Bragg peak is seen in the curves at high pressure. Only a slight inflection in the scattering curve is visible, centered at $Q_0 = 0.126$ Å$^{-1}$. The solid lines in Fig. 3, for pressures above 5.0 MPa, are the results of model calculations consisting of SLVs, SSs, and simple sheet-like structures. Initial attempts to model the data as SLVs + SSs or SLVs + sheets, alone,

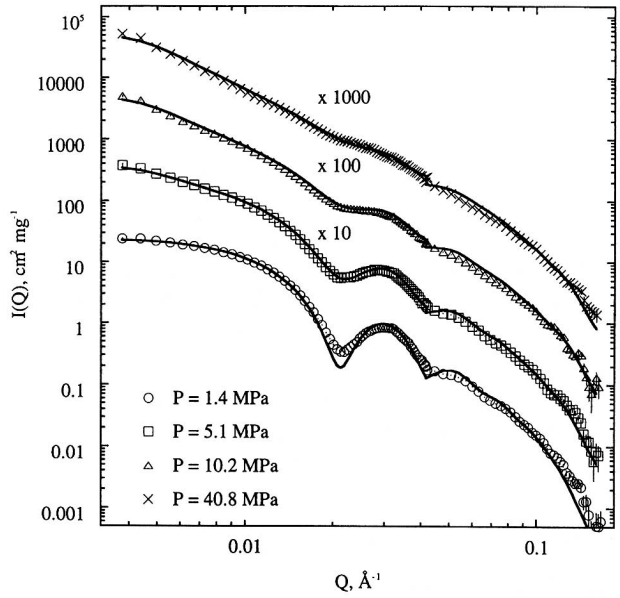


**Fig. 3.** Measured line shapes of the CG/EYPC system as a function of pressure ar $T = 37$°C.

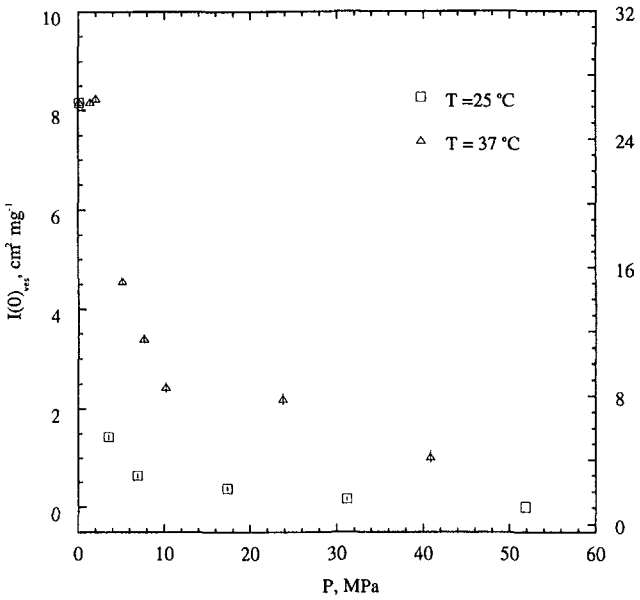


**Fig. 4.** Zero-angle intensity contribution from the SLV phase as a function of $P$(□, $T = 25°C$—left axis; △, $T = 37°C$—right axis). The rapid decrease in the contribution is indicative of vesicle collapse.

failed, as while both models describe the data well in the low-$Q$ region, the former falls off too quickly and the latter too slowly in the region $Q > 0.012$ Å$^{-1}$. For all fits shown in Fig. 3, the radius of the vesicle was held constant at 170 Å and the thickness of the vesicle fixed at 40 Å. For the sheet-like structures, the best fits were obtained with a sheet thickness of 38 Å and $d = 50$ Å. Slightly better fits were obtained at the higher pressures by increasing the stack height of the SS phase from 6 to 10.

Figure 4 shows a plot of the zero-angle intensity contribution from the SLV phase as a function of pressure for both temperatures. In both cases, the contribution from the SLV phase decreased rapidly with increasing pressure, indicative of vesicle collapse. The finer steps in pressure at 37°C demonstrate the abrupt collapse clearly, as the SLV phase contribution decreased by 43% on raising $P$ from 2.0 to 5.0 MPa.

## 4. DISCUSSION

The observed pressure-dependent changes in the bile salt/EYPC particle morphology implies that PV work can be done on them. This provides insight into the factors that stabilize the particle shapes. At both tem-

peratures studied, evidence of vesicle collapse is apparent in the measured line shapes with increasing pressure. The collapse of the vesicles suggests that the applied pressure exceeded the effective pressure of the vesicles as described previously. If we model the effective pressure according to the Y-L equation, using a nominal value of 50 $mN \cdot m^{-1}$ for $\gamma'$ and an average value of $R$ of 159 Å, we calculate a $\Delta p$ of $\sim 6.3$ MPa. As shown in Fig. 4, this is very close to the pressure at which the contribution to the overall scattering from the vesicle phase becomes insignificant. Thus, even if it is unlikely that a hydrostatic or osmotic pressure gradient exists in vesicles, the shape is stabilized by an apparent pressure that behaves something like that predicted by the Y-L equation.

At pressures above 6.9 MPa, we see the formation of ribbon-like particles at 25°C. The ribbon-like structure can arise from discrete particles or from defects in lamellar layers, as are found in some other liquid crystalline systems [13]. In either case, the formation of such anisotropic structures would require a redistribution of the bile salt from the interior of the bilayer to the edges, thus stabilizing the ribbon phase by shielding the EYPC tails from contact with water. The anisotropic form of the ribbon phase indicates a strong tendency of the bile salt to associate with the EYPC tail as opposed to being in solution. Such a pressure-driven rearrangement implies a significant volume change associated with the removal of bile salt from the bilayer interior to the bilayer edge. This arrangement is not unprecedented, as in the ribbon phase of the potassium palmitate/potassium laurate/water system [14], the shorter-tailed monomers (potassium laurate) are found to segregate to the exterior surfaces of the ribbons.

The presence of bile salt at the ribbon edges is consistent with the molar ratio of BS to EYPC. The lack of a ribbon phase in the CG/EYPC system at 37°C may be anticipated with an increased solution solubility of the bile salt component at the higher temperature [15]. With the bile salt preferring to be associated with the water phase, the ribbon-like structures cannot be supported, leading to the observed infinite sheet-like structures. Also, at the higher temperature, there is likely an increase in membrane fluctuations, which can prevent stacking.

## 5. CONCLUSION

Using small angle neutron scattering, we have studied the aggregate structure in the isotropic phase of the CG/EYPC system as a function of pressure. At $T = 25°C$, upon increasing the external hydrostatic pressure, a transition from an isotropic phase of discrete particles to an ordered phase was observed. At the highest pressures investigated, the CG/EYPC was found to transform to a ribbon phase. At $T = 37°C$, a similar behavior was

seen with increasing pressure. However, no ribbon phase was found at the highest pressure studied. The observed collapse of the SLVs with increasing pressure is consistent with the Y-L model. Additional measurements are needed in order to clarify the nature of the pressure gradient across the curved surfaces of the colloids formed by the GC/EYPC system.

## 6. ACKNOWLEDGMENTS

This work was supported by Laboratory Directed Research and Development Funds conducted under the auspices of the United States Department of Energy at the Manuel Lujan Jr. Neutron Scattering Center, Los Alamos Neutron Science Center of the Los Alamos National Laboratory, which is supported by the Office of Basic Energy Sciences of the United States Department of Energy under Contract W-7405-Eng-36 to the University of California. This work benefited from the use of NG3SANS at the National Institutes of Standards and Technology (NIST). This work also benefited from the use of the Intense Pulsed Neutron Source (IPNS) at Argonne National Laboratory. This facility is funded by the U.S. Department of Energy, BES-Materials Science, Under Contract W-31-109-Eng-38. We thank Dr. B. Hammouda (NIST), and Dr. P. Thiyagarajan (IPNS) for expert help in carrying out these measurements and Prof. H. Alkan-Onyuksel of the Department of Pharmaceutics and Pharmacokinetics, University of Illinois, Chicago for samples.

## REFERENCES

1. S. A. Safran, P. A. Pincus, D. Andelman, and F. C. MacKintosh, *Phys. Rev. A* **43**:1071 (1991).
2. R. Bruinsma, M. Goulian, and P. Pincus, *Biophys. J.* **67**:746 (1994).
3. M. M. Kozlov and V. S. Markin, *J. Phys. (France)* **51**:559 (1990).
4. J. Israelachvili, *Intermolecular and Surface Forces* (Academic Press, London, 1985).
5. O. Zhong-can and W. Helfrich, *Phys. Rev. A* **39**:5280 (1989).
6. C. Tanford, *Proc. Natl. Acad. Sci. USA* **76**:3318 (1979).
7. S. H. White, *Proc. Natl. Acad. Sci. USA* **77**:4048 (1980).
8. S. E. Feller and R. W. Pastor, *Biophys. J.* **71**:1350 (1996).
9. F. Jahnig, *Biophys. J.* **71**:1348 (1996).
10. R. P. Hjelm, *J. Appl. Cryst.* **21**:618 (1988).
11. R. P. Hjelm, H. Alkan, and P. Thiyagarajan, *Mol. Cryst. Liq. Cryst.* **180A**:155 (1990).
12. S. Corradini, G. Arancia, A. Calcabrini, P. Guardia, L. Baiocchi, A. Nistri, L. Giacomelli, and M. Angelico, *J. Hepatol.* **22**:642 (1995).
13. M. C. Holmes, M. S. Leaver, and A. M. Smith, *Langmuir* **11**:356 (1995), and references therein.
14. G. Chidichimo, A. Golemme, J. W. Doane, and P. Westerman, *J. Chem. Phys.* **82**: 536 (1985).
15. J. T. Mang and R. P. Hjelm, *Mol. Cryst. Liq. Cryst.* **299**:439 (1997).